



## On low-cost GNSS observables under different grades of antennas: Receiver-related biases and RTK results

Luohong Li<sup>a,b</sup>, Yunbin Yuan<sup>a,\*</sup>, Pengfei Zhang<sup>a,b</sup>

<sup>a</sup> State Key Laboratory of Geodesy and Earth's Dynamics, Innovation Academy for Precision Measurement Science and Technology, Chinese Academy of Sciences, Wuhan, China

<sup>b</sup> College of Earth and Planetary Sciences, University of Chinese Academy of Sciences, Beijing, China

### ARTICLE INFO

#### Keywords:

Receiver-related biases  
Low-cost receivers  
Single differenced RTK

### ABSTRACT

Low-cost receivers are becoming mainstream devices for providing positioning, navigation and timing (PNT) services that are accessible to the public. In contrast to existing advances, it is inappropriate for less-rigorous functional models and rough systemic error models, including the unknown characteristics of receiver-related biases (RRB) caused by internal hardware and the indefinite impact of an external antenna, to restrain the development of low-cost global navigation satellite system (GNSS) receivers. In this work, a comparative analysis was conducted to assess the respective effects of the internal hardware and an external antenna on low-cost receiver observables. We reparameterized a single-differenced geometry-based functional model and adopted a least squares filtering method to estimate RRB, including inter system biases (ISB), differential code biases (DCB), differential phase biases (DPB). First, an abnormal phenomenon was reported that the C099-F9P receiver showed better performance than the Trimble receiver on RRB when a U-blox ANN-MB antenna was used. Second, comparing the DCB and the DPB results, we found that the negative effect of the external antenna on the code observables is stronger than that on the phase observables. The standard deviation (STD) of the L1-L2 and E1-E5b DCB from the C099-F9P receiver reach 0.160 and 0.129 m, respectively, when the ANN-MB antenna is used. When connected to a higher-grade antenna, the low-cost receivers show DCB estimates stability similar to the Trimble receivers, where the L1-L2 and E1-E5b DCB STDs can reach 0.078 and 0.076 m, respectively. Third, it should be noted that the L1-L2 and E1-E5b DCB will change if a low-cost receiver restarts or is powered off. Fourth, of the DPB STDs of the low-cost and Trimble receivers connected to three different grades of antennas maintain agreement and reach 0.007 cycles or better. The phase observables can be free from the effect of the antenna in short-term case. Above all, the comparison results illustrate that low-cost GNSS receivers have the potential for high-precision applications and achieve an accuracy level and ability similar to high-grade receivers in mass applications when a survey-grade or higher-quality antenna is equipped.

### 1. Introduction

The recent advances in low-cost global navigation satellite system (GNSS) chipsets and smart devices, progress in processing algorithms and hardware technology, along with their preponderance of miniaturization and feasibility, are catalyzing an expansion of conventional satellite navigation to novel areas for mass service [1]. It is no doubt that low-cost receivers have potential to achieve the high GNSS position service [2,3]. In particular, it has been shown that existing low-cost

devices might be successfully employed in precise applications such as positioning and time transfer [4], integrated use with Inertial Navigation System [5], deformation monitoring [6] and atmospheric modeling [7–9]. With these advancements, low-cost receivers can provide accessible positioning, navigation, and timing (PNT) information for public and may now be considered a mature complement to high-grade receivers in emerging PNT applications [10,11].

Compared with increasing mass-market demand, less-rigorous functional models are restraining the development of low-cost GNSS

**Abbreviations:** PNT, Positioning, Navigation and Timing; GNSS, Global Navigation Satellite System; ISB, Inter system Biases; DCB, Differential Code Biases; DPB, Differential Phase Biases; RRB, Receiver-Related Biases; PPP, Precise Point Positioning; VTEC, Vertical Total Electron Content; SDB, Signal Distortion Biases; RTK, Real-Time Kinematic; SD, Single Differenced; DD, Double Differenced.

\* Corresponding author.

E-mail address: [yybgps@apm.ac.cn](mailto:yybgps@apm.ac.cn) (Y. Yuan).

<https://doi.org/10.1016/j.measurement.2023.112771>

Received 12 November 2022; Received in revised form 17 March 2023; Accepted 20 March 2023

Available online 23 March 2023

0263-2241/© 2023 Elsevier Ltd. All rights reserved.

receivers, such as unmodeled receiver-related biases caused by hardware defects [12]. Meanwhile, a stochastic model is unknown since it is related to many internal and external factors, such as the antenna and internal hardware of a receiver [13,14]. It is crucial and urgent to model receiver-related biases (RRB) and obtain a refinement relationship between observable quality and the related hardware for low-cost receivers, because the available RRB models and mitigation methods have only been developed for geodetic receivers, especially precise point positioning (PPP) algorithm [15,36]. For miniaturization and feasibility, patch antennas are usually combined with low-cost receivers, which is a new challenge for the original functional models and RRB characters [16]. Additionally, Zhao et al. found that receiver clock jumps often occur in low-cost GNSS observables because the receiver clock is Temperature-Compensated Crystal Oscillators (TXCO) and needs to reset itself to synchronize with the standard system time [17]. As for clock jump and cycle slips, Momoh et al. proposed an algorithm capable of detecting and correcting receiver clock jumps at millisecond and microsecond levels and cycle slips for a single-frequency receiver [18]. In addition, Gong et al. estimated signal distortion biases (SDB) from GNSS observations from the MGEX geodetic network and found that SDB are originated from satellite and receiver hardware delays and the biases are stable over a short time [19]. It should be calibrated with the update of receiver brands and models and it is inferred that the negative effect may be more significant for low-cost devices. If we cannot address and model the biases properly, they will impair the functional model and have a negative effect on stochastic modeling [12,20]. In the tightly coupled model, the inter-system biases (ISB) should be considered because a pivot satellite is chosen and shared among all tracked systems and conduct inter-system double-differencing on the overlapping carrier frequencies [21–24]. The ISB characteristics will obviously affect the performance of ambiguity resolution (AR) with low-cost receiver [25]. It should be noted that the phase and code ISB are related to the receiver type, firmware version and selected overlapping frequency. It has long been recognized that low-cost observables have the potential to retrieve vertical total electron content (VTEC) with Single frequency (PPP) approach [35]. However, receiver differential code biases (DCB) have an adverse impact on sensing VTEC [26,27,34,36]. So we need handle receiver DCB well when we model VTEC with low-cost devices. Overall, deficient functional model and RRB knowledge occurs often in low-cost GNSS devices, blocking their extensive application, such as PPP and PPP-RTK application.

Although the above works have investigated the GNSS signal quality and RRB of geodetic receivers, a comparative analysis of geodetic receivers and low-cost observables and the impact of external antennas on low-cost observables is lacking. Further attention should be given to improving the RRB model of low-cost receivers and investigating the relationship between the RRB characters and low-cost hardware and external antennas configurations. Once these problems are addressed, the refined function model and RRB characteristics will shift low-cost GNSS receivers toward high-precision applications.

The unknown impact of low-cost external antenna and internal hardware on observables has been the main concern and constraint for low-cost GNSS data processing. With a zero-length baseline that is free from other external factors, it is unique to quantify the impact of external antennas on RRB and the quality of observables from low-cost and high-grade receivers, which will provide new knowledge for handling RRB in low-cost receivers.

A comparative analysis between low-cost receivers and geodetic receivers of the signal quality and character of the RRB is systematically studied in this paper under a zero-length baseline setup when connected with different external antennas. The paper is organized as follows. In Section 2, we present a between-receiver single-differenced [28] RTK functional model and derive a full-rank model after the reparameterization procedure. A LSF method is adopted to enable the successive estimation of DPB and correctly fix ambiguity. In Section 3, we first present the experimental setup and processing strategies and the

characteristics of the RRB estimates of low-cost and high-grade receivers are compared, including the clock offset, ISB, DCB and DPB. Additionally, the float results and fixed solutions are determined with few remarkable phenomena reported. The corresponding position performance of the Single Differenced (SD) Real-Time Kinematic (RTK) model under six typical cases are discussed in detail. The conclusion was drawn in Section 4.

## 2. Methodology

### 2.1. The single-differenced functional model

In general, GNSS stochastic modeling should be based purely on random errors, and RRB estimation also needs to be free from external noise. Hence, an ultrashort baseline (zero-length baseline in our case) is usually used to eliminate systematic biases, for instance, multipath, tropospheric, ionospheric errors and so on, from external sources. The core of this work is to provide a new approach to the evaluation and modeling of RRB, which may be contaminated by noise from external factors. In contrast, a double differenced (DD) model excludes the impact of RRB, but the RRB are retained in an SD model. Hence, the SD model is preferred in this work.

Eliminating the systematic errors and atmospheric effects on zero-length baselines, a rank-deficient RTK model using an SD code and phase observations on frequency  $j$  of two constellations can be given as [20]:

$$\Delta\phi_{br,j}^{sc} = \Delta\rho_{br}^{sc} + \Delta dt_{br} - \lambda_j^c \Delta a_{br,j}^{sc} + \lambda_j \Delta \delta_{br,j}^c + \varepsilon_{\Delta\phi_{br,j}^{sc}} \quad (1)$$

$$\Delta p_{br,j}^{sc} = \Delta\rho_{br}^{sc} + \Delta dt_{br} + \Delta d_{br,j}^c + e_{\Delta p_{br,j}^{sc}} \quad (2)$$

where “ $\Delta$ ” denotes the operators between receiver differences; superscript “ $sc$ ” denotes the tracked satellites  $s$  of GNSS constellation  $c$  ( $G$  represents GPS and  $E$  represents Galileo); subscripts “ $b$ ” and “ $r$ ” are the base receiver and rover receiver, respectively;  $\Delta\phi_{br,j}^{sc}$  and  $\Delta p_{br,j}^{sc}$  are the SD phase and code observable in units of meters, respectively;  $\delta t_{br,j}$  are the SD receiver clock errors;  $\rho$  is the receiver-satellite range;  $a_{br}^{sc}$  and  $\lambda_j^c$  are the SD integer ambiguity parameters in units of cycle and wavelength at the corresponding frequency  $j$ , respectively;  $\varepsilon_j^c$  and  $d_j^c$  are the receiver phase and code bias, respectively, which are treated as an error common to a complete GNSS constellation  $c$ ; and  $\varepsilon$  and  $e$  are the measurement noises of the phase and code observable, respectively. Note that the satellite-specific errors, including the time offset between different GNSS, are eliminated when creating SD observations, and  $\delta_j^c$  is in units of cycle.

Clearly, the SD observation equations are not a full-rank system [29]. The rank deficiency for the SD functional model comes from two sources: one is the rank defects between the receiver clock and code/phase delay columns, and the other is the column dependency between the phase delays and ambiguities [30]. It is common practice to eliminate these rank deficiencies by selecting an S-basis for each constellation.

To overcome the rank defects of the first type, we choose to fix the hardware delays on the first frequency of the GPS system, which are introduced in [31]. Then, we have only the rank defects between the phase biases and ambiguities, which are solved by fixing the SD ambiguities of one reference satellite per constellation. Therefore, the reparameterized phase bias  $\lambda_j \delta_j^c$  at an arbitrary frequency will absorb the SD ambiguity parameter of the selected reference satellite on the corresponding frequency, which leads to reparameterized ambiguities having a DD form. Then, the ambiguities retain an integer characteristic and are easy to fix using the least-squares ambiguity decorrelation adjustment (LAMBDA) method [32]. When we address the rank defects in the original model using the above two reparameterized strategies, the form of the parameters has been changed, and the reparameterized parameters will enable the model to be full-rank and facile. The

reparameterized parameters are as follows, in which ‘ $\Delta$ ’ is omitted for simplicity.

**Table 1** presents the reparameterized important parameters to address the rank defects in the model. Parameters whose subscript is “ $br$ ” are regarded as those related to the receiver, which can be treated carefully and estimated in the model. For simplicity and clarity, the subscript “ $br$ ” is omitted from the following symbols. The reparameterized parameters  $\tilde{d}_1^E$ ,  $d_1^E$ ,  $\tilde{d}_2^c$ ,  $\delta_1^c$ , and  $\tilde{\delta}_2^c$  denote the receiver clock offset with code biases  $d_1^G$ , receiver code ISB, receiver DCB of constellation  $c$ , receiver phase biases on the first frequency of constellation  $c$ , and receiver DPB in practical physical meaning, respectively.  $\tilde{a}_j^c$  are DD integer ambiguities. It should be noted that because  $d_1^E$  actually refers to the ISB parameter between GPS and Galileo, we use “ISB” to replace  $\tilde{d}_1^E$  to clearly show the actual meaning of the parameter.

After the above reparameterized process, the full-rank RTK model using an SD code and phase observations on frequency  $j$  of two constellations can be given as:

$$E \left( \begin{bmatrix} \Delta\phi_{br}^{sg} \\ \Delta p_{br}^{sg} \\ \Delta\phi_{br}^{se} \\ \Delta p_{br}^{se} \end{bmatrix} \right) = A \bullet X \quad (3)$$

$$A = \begin{bmatrix} e_2 \otimes A_n & e_{2n} & K^G & H^G \\ e_2 \otimes A_n & e_{2n} & \begin{bmatrix} 0_n \\ e_n \end{bmatrix} & \\ e_2 \otimes A_m & e_{2m} & & K^E & H^E \\ e_2 \otimes A_m & e_{2m} & & e_{2m} & \begin{bmatrix} 0_m \\ e_m \end{bmatrix} \end{bmatrix} \quad (4)$$

and the parameters to be estimated  $X$  are presented as follows:

$$X = \left[ \Delta x^T \quad d_1^T \quad \tilde{d}_2^{GT} \quad \tilde{\delta}^{GT} \quad \tilde{A}^{sgT} \quad ISB^T \quad \tilde{d}_2^{ET} \quad \tilde{\delta}^{ET} \quad \tilde{A}^{seT} \right]^T \quad (5)$$

where ‘ $E$ ’ denotes an expectation operators;  $\Delta\phi^{sg} = [\Delta\phi_{br,1}^1, \dots, \Delta\phi_{br,1}^n, \Delta\phi_{br,2}^1, \dots, \Delta\phi_{br,2}^n]^T$  and  $\Delta p^{sg}$  has the same structure;  $\tilde{\delta}^E = [\tilde{\delta}_{br,1}^E, \tilde{\delta}_{br,2}^E]^T$ ;  $\tilde{A}^{sg} = [0, \tilde{a}_{br,1}^2, \dots, \tilde{a}_{br,1}^n, 0, \tilde{a}_{br,2}^2, \dots, \tilde{a}_{br,2}^n]^T$ ;  $n$  is tracked satellites in GPS constellation and  $m$  for Galileo;  $A_s$  is a  $3 \times s$  design matrix of baseline components in three directions  $\Delta x = [dx, dy, dz]^T$ ;  $0_s$

**Table 1**  
Estimable unknown parameters and their interpretation for the SD model.

Notation and interpretation	Estimable parameter
$\tilde{d}_1 = dt + d_1^G$	Receiver clock with code biases at the first frequency
$\tilde{d}_j^G = d_j^c - d_1^G$	Receiver DCB in GPS, where $j = 2$
$\lambda_1^G \delta_1^G = \lambda_1^G \delta_1^G - d_1^G + \lambda_1^G a_1^{1g}$	Receiver phase bias in GPS of the first frequency
$\lambda_j^G \delta_j^G = \lambda_j^G \delta_j^G - \lambda_1^G \delta_1^G + \lambda_j^G a_j^{1g} - \lambda_j^G a_1^{1g}$	Receiver DPB in GPS, where $j = 2$
$d_1^E = dt^E + \tilde{d}_1^E - dt - d_1^G$	Receiver ISB with code biases at the first frequency
$\tilde{d}_j^E = d_j^E - d_1^E$	Receiver DCB in Galileo
$\lambda_1^E \delta_1^E = \lambda_1^E \delta_1^E - d_1^E + \lambda_1^E a_1^{1e}$	Receiver phase bias in Galileo of the first frequency
$\lambda_j^E \delta_j^E = \lambda_j^E \delta_j^E - \lambda_1^E \delta_1^E + \lambda_j^E a_j^{1e} - \lambda_1^E a_1^{1e}$	Receiver DPB in Galileo, where $j = 2$
$\lambda_j^c \tilde{a}_j^c = \lambda_j^c a_j^c - \lambda_j^c a_1^c$	Reparameterized double-differenced (DD) integer ambiguities

is an s-column vector of all zeros;  $e_s$  and  $I_s$  are the s-column vector with all ones and  $s \times s$  identity matrix, respectively;  $\Lambda_s = [0_{(s-1) \times 1}, I_{s-1}]$ ; and “ $\otimes$ ” is the Kronecker product operator.  $K^G = \begin{bmatrix} \lambda_1^G \\ \lambda_2^G \end{bmatrix} \otimes e_n$ ;  $K^E = \begin{bmatrix} \lambda_1^E \\ \lambda_2^E \end{bmatrix} \otimes e_m$ ;  $H^G = \begin{bmatrix} \lambda_1^G \\ \lambda_2^G \end{bmatrix} \otimes \Lambda_n$ ;  $H^E = \begin{bmatrix} \lambda_1^E \\ \lambda_2^E \end{bmatrix} \otimes \Lambda_m$ . Once the rank defects in original model have been addressed, we have a single-epoch full-rank model. We can capture the characters of receiver related biases with epoch-wise estimate.

## 2.2. The least squares filtering method

However, a problem exists in the parameter estimation process when we continuously observe the GNSS. In the DPB estimable forms  $\lambda_j^G \tilde{a}_j^G = \lambda_j^G \delta_j^G - \lambda_1^G \delta_1^G + \lambda_j^G a_1^{1g} - \lambda_j^G a_1^{1g}$  and  $\lambda_j^E \tilde{a}_j^E = \lambda_j^E \delta_j^E - \lambda_1^E \delta_1^E + \lambda_j^E a_1^{1e} - \lambda_j^E a_1^{1e}$ , the datum ambiguities  $\lambda_j^G a_1^{1g} - \lambda_1^G a_1^{1g}$  and  $\lambda_j^E a_1^{1e} - \lambda_1^E a_1^{1e}$  correspond to the reference satellites  $1_G$  and  $1_E$ . It is common during long-term low-cost observable campaigns to lose lock on the reference satellites, the reference satellites become blocked or cycle slip occurs. In such circumstances, abrupt jumps caused by reference ambiguity will be introduced in the epochwise DPB estimates and impede the restoration of their characteristics.

Least squares filtering is a suitable method for the maintenance of the referenced ambiguity and the continuous epochwise estimation of DPB, which is a filtering method derived from the perspective of generalized least squares. The Kalman filter and the least-squares estimator are algebraic equivalence [33]. The Kalman filter and the least square filter all need the approximated value of model parameters in nonlinear problems. But the LSF can predict partial (optional) parameters in time update step, instead of all parameters. Meanwhile, the formula and algorithm is simple and easy to implement [17].

Thus, maintaining a reasonably compatible datum is important and pressing in this model. We noted that the reparameterized ambiguities are in DD form, which can be specified using an integer with the LAMBDA method. The integer ambiguities  $\lambda_j^c a_j^c$  are passed on, enhancing the success rate of resolving ambiguities in the next epoch. Moreover, the DD ambiguities  $\lambda_j^c a_j^c$  and the datum ambiguities  $\lambda_j^E a_1^{1e}$  can be transferred to the next epoch. Even if a reference satellite is no longer visible, it can still serve as a datum. There is a fault in such a model, which is that the successive DPB estimation requires continuous ambiguity parameter fixing. However, for a zero-length or short baseline, we consider this task to be easy in short-term case.

For the detailed algorithm, we first recall the basic least squares principle. The least squares form of formula (12) can be rewritten as follows:

$$E(Y) = E \left( \begin{bmatrix} \Delta\phi_{br}^{sg} \\ \Delta p_{br}^{sg} \\ \Delta\phi_{br}^{se} \\ \Delta p_{br}^{se} \end{bmatrix} \right) = A \bullet X \quad (6)$$

$$B = \begin{bmatrix} & I_{n_G} & \\ & & I_{n_E} \end{bmatrix} \quad (7)$$

where  $\tilde{A}^{sg}$  and  $\tilde{A}^{se}$  are the ambiguity parameters and are a submatrix of  $X$ . The ambiguities from  $X$  can be obtained from  $\tilde{A} = [\tilde{A}^{sgT} \quad \tilde{A}^{seT}]^T = B \cdot X$ .

The core of LSF is to describe the change process of the parameters to be estimated between adjacent epochs through a state equation and realize the prediction of the parameters to be estimated and their

variance information. The implementation process includes three steps: state prediction, reconstruction of the observation equations and parameter estimation. For simplicity and clarity, we use the subscript  $i$  to refer to the epoch, and a parameter with subscript  $i$  denotes the parameter at epoch  $i$ .

The state prediction is as follows:

$$\tilde{A}_i = \Phi_{i|i-1} \tilde{A}_{i-1} + \xi_i \quad (8)$$

$$\hat{D}_{\tilde{A},i} = \Phi_{i|i-1} \hat{D}_{\tilde{A},i-1} \Phi_{i|i-1}^T + D_{\xi_i} \quad (9)$$

where  $\tilde{A}_i$  is the predicted vector of the ambiguity parameters fixed at epoch  $i$ , and the predicted variance of  $\tilde{A}_i$  is  $\hat{D}_{\tilde{A},i}$ ;  $\Phi_{i|i-1}$  is the transition matrix of the ambiguity parameters between epoch  $i$  and epoch  $i-1$ ;  $\xi_i$  is the process noise, and the prior (presumptive) variance of  $\xi_i$  is  $D_{\xi_i}$ . It should be noted that  $\tilde{A}_{i-1}$  are the fixed ambiguities of the previous epoch and are passed to the current epoch, where the corresponding ambiguities will be canceled if a cycle slip is detected or the satellite is dropped.

The reconstruction of the observation equations is as follows:

$$\check{X}_i [A_i \quad B_i]^T \check{X}_i = \begin{bmatrix} Y_i \\ \tilde{A}_i \end{bmatrix} \quad (10)$$

$$D \begin{bmatrix} Y_i \\ \tilde{A}_i \end{bmatrix} = \begin{bmatrix} D_{Y_i Y_i} & \hat{D}_{\tilde{A},i} \\ \hat{D}_{\tilde{A},i} & \hat{D}_{\tilde{A},i} \end{bmatrix} \quad (11)$$

where  $A_i$ ,  $Y_i$  and  $D_{Y_i Y_i}$  denote the design matrix, observable vectors and their variance matrix, respectively, and 'D' denotes the dispersion operators.

The parameter estimation is as follows:

$$\check{X}_i = \left( A_i^T D_{Y_i Y_i}^{-1} A_i + B_i^T \hat{D}_{\tilde{A},i}^{-1} B_i \right)^{-1} \left( A_i^T D_{Y_i Y_i}^{-1} Y_i + B_i^T \hat{D}_{\tilde{A},i}^{-1} \tilde{A}_i \right) \quad (12)$$

$$\check{D}_{X,i} = \left( A_i^T D_{Y_i Y_i}^{-1} A_i + B_i^T \hat{D}_{\tilde{A},i}^{-1} B_i \right)^{-1} \quad (13)$$

We adopt LSF in this model, and only the fixed DD ambiguities  $\tilde{A}_i$  are regarded as the virtual observation value and the measured value of the current epoch for simultaneous adjustment to obtain the parameter estimation and variance information of the current epoch. Therefore, the model has better strength and maintains the DD ambiguities fixed correctly, which is helpful for other parameters, such as the DPB and DCB.

### 3. Results and summary

#### 3.1. Experimental setup

We deployed four multi-GNSS receivers, including two Trimble Alloy geodetic receivers (APM1 and APM2) and two U-blox C099-F9P boards (F9P1 and F9P2) equipped with a U-blox ZED-F9P chip, on the roof of the No. 3 building of the Innovation Academy for Precision Measurement Science and Technology in Wuhan (114.4° E, 33.6° N in WGS84), which is an open-sky environment. Trimble Alloy receiver are a famous high-precision receiver type. The C099-F9P GNSS module is a typical low-cost receiver, which is capable of multi-frequency multi-GNSS RTK and costs less than US \$300. The firmware version of the two Trimble receivers is set to version 5.22. All four receivers can track dual-frequency GPS (L1/L2) and Galileo (E1/E5b) signals. We design two groups of zero-length baseline, including F9P0-F9P1 pair (F9P) and APM-AOMB pair (APM). The four receivers were connected to a external antenna via a 4-way power divider. It is noted that all four receivers receive the same signal from the same antenna simultaneously, which is comparable for low-cost and high-grade receivers to analyze the negative effect of internal hardware and the external antenna on the

GNSS observables. It is feasible to study the RRB characters under zero-baseline mode because they can reflect the quality of the satellite signal since the common errors can be eliminated completely, such as multipath errors. The detailed configuration between receivers and antennas in this experiment is presented in Fig. 1. Three typical antennas are used in our campaign, including the ANN-MB antenna (low-cost grade), Comnav AT360 (survey-grade), and Trimble GNSS-Ti Choke Ring (geodetic-grade). For simple and clarity, we used 'UBX', 'CMN' and 'TRM' referring to U-blox ANN-MB, Comnav AT360 and Trimble GNSS-Ti Choke Ring antenna.

The elevation-dependent weighting function for the high-grade receivers and the C/N0 weighting function for the low-cost receivers were used. The standard deviation (STD) values of the undifferenced phase and code were 3 mm and 0.3 m, respectively. The empirical precision of the SD observables was obtained by multiplying the precision of the undifferenced observables by  $\sqrt{2}$ . A ratio test was used to determine whether the integer ambiguities were resolved correctly, and the traditional threshold of 3.0 was used in the test. The reference coordinate is calculated by CSRS online service with the four-day 30 s interval observation from the Trimble receivers and CSRS is based on GPS-only precise point positioning with ambiguity resolution (PPP-AR). The NRCan reported that the ratio of fixed ambiguities exceeds 98% and the precision of reference coordinate under 95% confidence achieved 1–2 cm.

Detailed information on the six groups of dataset is listed in Table 2. The different antenna and receiver type configurations during different durations are presented. The number of tracked GPS + Galileo satellites during the measurement campaign are over around 10. It is common that low-elevation satellites are measured discontinuously. The cutoff elevation angle of the satellites is set to 10°. It should be noted that the C099-F9P boards often lack the observables of the second frequency or part phase observables suddenly due to low-cost hardware. We enable the low-cost devices powered on and record the data intermittently during the campaign.

#### 3.2. Clock and ISB

Since zero-length baseline tests were conducted for the low-cost boards and Trimble receivers, the low-cost and high-grade receivers are compared with an emphasis on RRB, which may provide new information and evidence for understanding the biases of low-cost boards. It is anticipated that the handling of RRB may promote the use of low-cost GNSS devices for high-precision applications.

Figs. 2 and 3 show the estimates of the receiver clock and ISB between GPS and Galileo from the Trimble Alloy receiver pair (top) and U-blox F9P receiver pair (bottom) in the three datasets. The irregular changes in the clock are aggravated while the receivers are connected to a less expensive antenna, which is obviously shown in Fig. 2(a) and Fig. 2(d). Notably, receiver clock jumps occur when the receivers. In contrast to the clock offset of the Trimble receivers, the clock offset of the low-cost receivers show instability characteristics. It is more probable that the receiver clock error from the Trimble is corrected for the clock error, and that is not the case for the U-blox. In addition, we observed that clock shaking occurs almost simultaneously because the four receivers are connected to the same U-blox ANN-MB antenna concurrently. It can be observed that the U-blox ANN-MB clock series are much noisier than the others. We concluded that the jump and noise of the low-cost receiver clock may be affected by the external antenna. When we are concerned with the clock offset of low-cost receivers, the clock jumps notably, which is caused by a poor-quality crystal oscillator [17]. This is a disadvantage for its use in high-precision applications.

When comparing the results in Fig. 3, which shows the code ISB of the Trimble Alloy receivers with different external antennas, we can see that the random characteristics of the code ISB are contaminated by noise caused by the external antenna hardware. The STD value of the

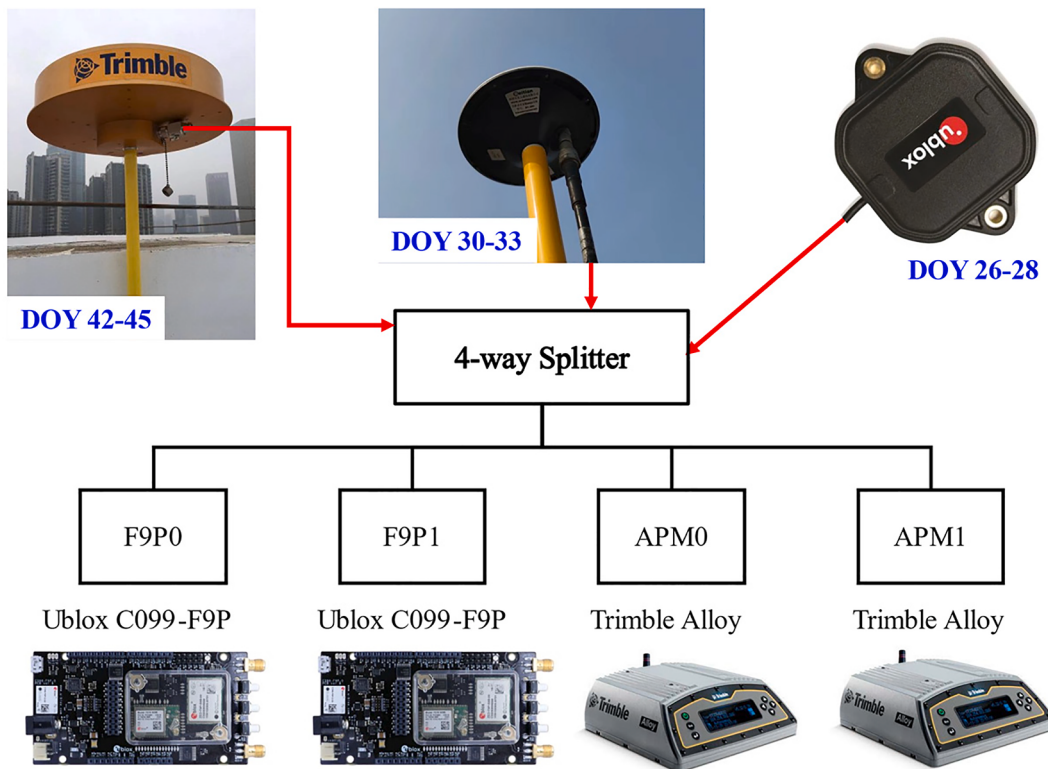


**Fig. 1.** Receiver and antenna setup during data collection.

**Table 2**  
Description of the receivers and antennas used in the datasets.

Dataset	Antenna type	Receiver type	Observation period	Sampling interval
No. 1	U-blox ANN-MB (low-cost grade)	Trimble Alloy pairs (APM1-APM2)	00:00:00-2:59:59 in DOY 026	1 s
No. 2	Comnav AT360 (survey-grade)	U-blox C099-F9P pairs	00:00:00-2:59:59 in DOY 031	1 s
No. 3	Trimble GNSS-Ti Choke Ring (geodetic-grade)	(F9P1-F9P2)	14:00:00-16:59:59 in DOY 043	1 s
No. 4	U-blox ANN-MB		DOY 026-028	30 s
No. 5	Comnav AT360		DOY 030-033	30 s
No. 6	Trimble GNSS-Ti Choke Ring		DOY 042-045	30 s

GPS-Galileo ISB of the Trimble receivers under UBX antenna is 3 times than that of the ISB under CMN antenna, while similar results from the low-cost receivers are also observed. Similar result can also be present in Fig. 4. It is concluded that the low-cost antenna will introduce additional noise to the observables and have a negative impact on the ISB. Meanwhile, the code ISB STD of the C099-F9P receivers connected to ANN-MB antenna shows a more stable character than that of the Trimble Alloy receivers in the same case. The noises from ANN-MB antenna will contaminate the observables from Trimble receivers and challenge the original functional model. In Table 3, the mean ISB values are  $-0.145$  and  $-0.022$  m for the low-cost and higher-grade antennas, respectively. The ISB of the Trimble receiver are close to the code ISB estimated by [15]. As for a long-term scale, we notice that ISB of Trimble receiver are steable and keep same over two weeks while the of low-cost receiver have varied in Fig. 4. It is obvious that the antenna of high grade bring less noise on ISB. When connected with the Comnav AT360 and Trimble

GNSS-Ti Choke Ring antennas, the Trimble receiver ISB is close to zero while the low-cost receiver ISB have a non-zero biases. The results indicate that we should consider the ISB of low-cost receivers in practice. Meanwhile, we find that the mean and STD ISB values are all small and similar between the U-blox F9P and the Trimble Alloy, which means that a stable ISB can be handled well in a tight combination model. It is recommended that real-time estimating for ISB is needed because the ISB may change over time and is not a constant.

### 3.3. DCB, phase biases and DPB

Figs. 5 and 6 show the L1-L2 and E1-E5b DCB results of the APM1-APM2 and F9P1-F9P2 pairs on DOYs 26, 31 and 43 of 2022. The statistical results of the DCB estimates of the APM1-APM2 and F9P1-F9P2 baselines are shown in Table 4. The DCB noise in the Trimble receivers + ANN + MB combination is still larger than that of the C099-F9P + ANN + MB combination.

When comparing the top panels of Figs. 5 and 6, showing the L1-L2 DCB and E1-E5b DCB estimated from APM1-APM2, we can see that the mean DCB values are almost unchanging in the Trimble Alloy receiver over 17 days, while the between-receiver DCB of the U-blox C099-F9P receivers pair have changed, although all receivers were restarted in the experiment. The L1-L2 DCB of APM1-APM2 is approximately  $-0.110$  m, and the E1-E5b DCB of APM1-APM2 is approximately  $-0.086$  m. We can conclude that the E1-E5b DCB of the Trimble Alloy receiver shows slightly more stability than the L1-L2 DCB, while the DCB of the low-cost U-blox C099-F9P receiver is unstable. The STD of the E1-E5b DCB on DOY 043 is 0.051 m. For the F9P1-F9P2 pair, the L1-L2 and E1-E5b DCB will change if the receiver is restarted.

As for DCB on a long-term scale, it can be observed that the values of receivers DCB are significant, but the intra-day stability is also noticeable. The receiver L1-L2 DCB varies in a day and Trimble receiver DCB will not jump over 2 weeks. The DCB of U-blox F9P will show jump and change in Figs. 7 and 8. The noise from hardware is larger than Trimble receivers on DCB. The E1-E5b DCB is stabler than L1-L2 DCB. It should

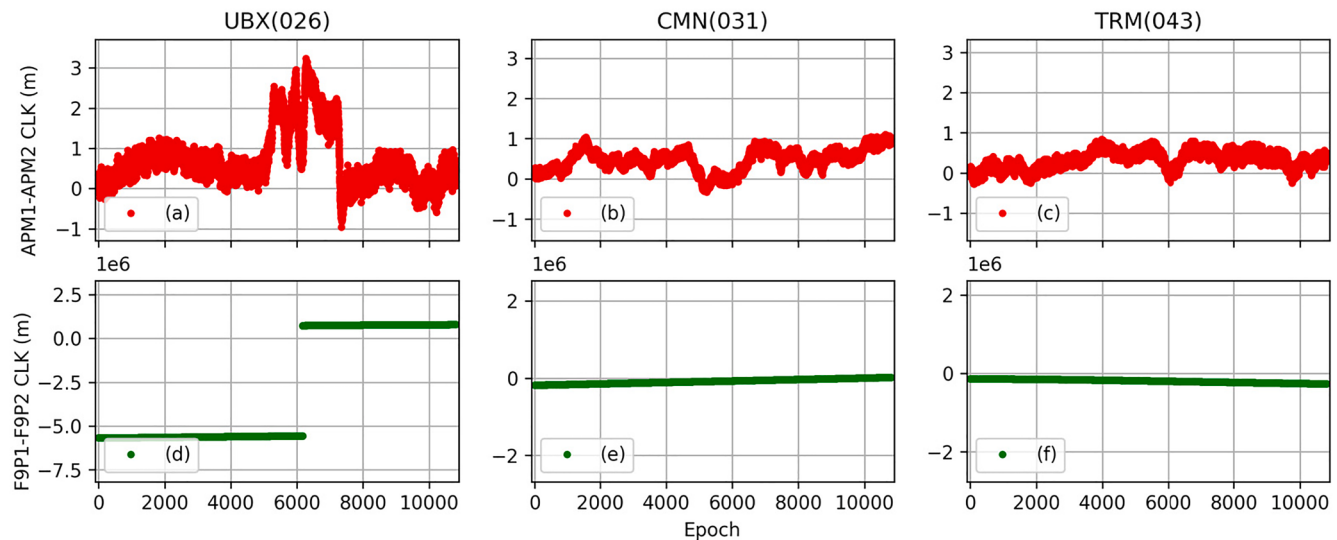


**Fig. 2.** Receiver clock offsets for the APM1-APM2 pair (top) and the F9P1-F9P2 pair (bottom) on DOYs 26, 31 and 43 of 2022.

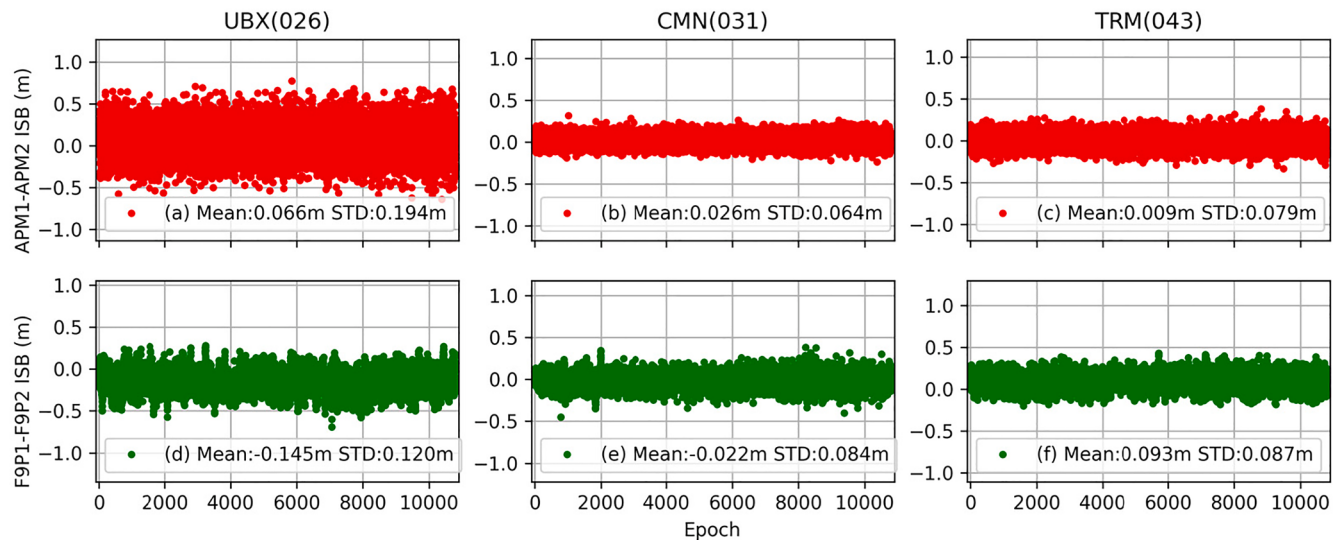


**Fig. 3.** Receiver ISB between GPS and Galileo for the APM1-APM2 pair (top) and the F9P1-F9P2 pair (bottom) on DOYs 26, 31 and 43 of 2022.

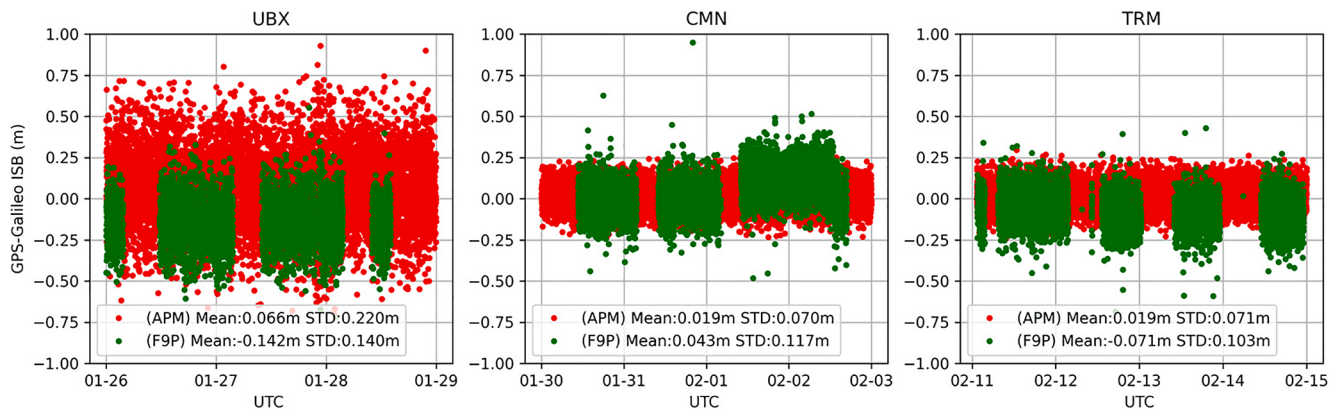


**Fig. 4.** Receiver ISB between GPS and Galileo for the APM1-APM2 pair (red) and the F9P1-F9P2 pair (green) on DOYs 26–28, 30–33 and 42–45 of 2022.

**Table 3**

ISB between GPS and Galileo of the zero-length baseline APM1-APM2 (Trimble Alloy receivers pair) and zero-length baseline F9P1-F9P2 (U-blox C099-F9P receivers pair) on DOYs 026, 031 and 043 in 2022.

Baseline	DOY	ISB (m)	
		Mean	STD
APM1-APM2	026 (UBX)	-0.066	0.194
	031 (CMN)	-0.026	0.064
	043 (TRM)	-0.009	0.079
F9P1-F9P2	026 (UBX)	-0.145	0.120
	031 (CMN)	-0.022	0.084
	043 (TRM)	-0.093	0.087

be noted that we can use low-cost receivers to obtain DCB estimates that are similar in precision to those of APM1-APM2, which is evidence to support the potential to achieve a high-precision VTEC model using low-cost receivers. The E1-E5b DCB and L1-L2 DCB have an obvious change in DOY 026 after we set F9P power off in Figs. 7 and 8. It is should be difficult for long-term VTEC modeling with low-cost receivers because their DCB are varied. We need to estimate and calibrate the DCB in advance for long-term VTEC modeling.

Different from DCB on code observables, the receiver DPB on phase observables will change because the DPB estimates vary with ambiguities. It is difficult to determine the DPB on a long-term scale, especially in low-cost GNSS receivers. So we do not take the long-term character of DPB and PB into consideration.

For the DPB, we first recall the DPB formulas,  $\lambda_j^G \tilde{\delta}_j^G = \lambda_j^G \delta_j^G - \lambda_1^G \tilde{\delta}_1^G + \lambda_j^G \mathbf{a}_j^{1_G} - \lambda_1^G \mathbf{a}_1^{1_G}$  and  $\lambda_j^E \tilde{\delta}_j^E = \lambda_j^E \delta_j^E - \lambda_1^E \tilde{\delta}_1^E + \lambda_j^E \mathbf{a}_j^{1_E} - \lambda_1^E \mathbf{a}_1^{1_E}$ . The estimated DPB are biased by the SD ambiguity  $\lambda_j^* \mathbf{a}_j^{1*} - \lambda_1^* \mathbf{a}_1^{1*}$ , where \* denotes a system index. In practice,  $\lambda_j^* \mathbf{a}_j^{1*} - \lambda_1^* \mathbf{a}_1^{1*}$  is a stable integer in our hypothesis, and the PB estimates are free from the impact of  $d_1^G$ . Figs. 9 and 10 show the L1-L2 and E1-E5b DPB estimates of APM1-APM2 (top) and F9P1-F9P2 (bottom) for the three types of antenna on DOYs 026, 031 and 043 of 2022. The detailed statistical results are shown in Table 5. It is noted that the scales of the Y-axis in Figs. 6 and 7 are different. To compare the L1-L2 and E1-E5b DPB on the same scale, the DPB estimates should be multiplied by the wavelength of the second frequency in the corresponding systems.

Two following conclusions can be drawn. First, according to the results of the different antennas, the DPB of the phase observables may be less affected by the antenna, although the STD of the biased DPB will

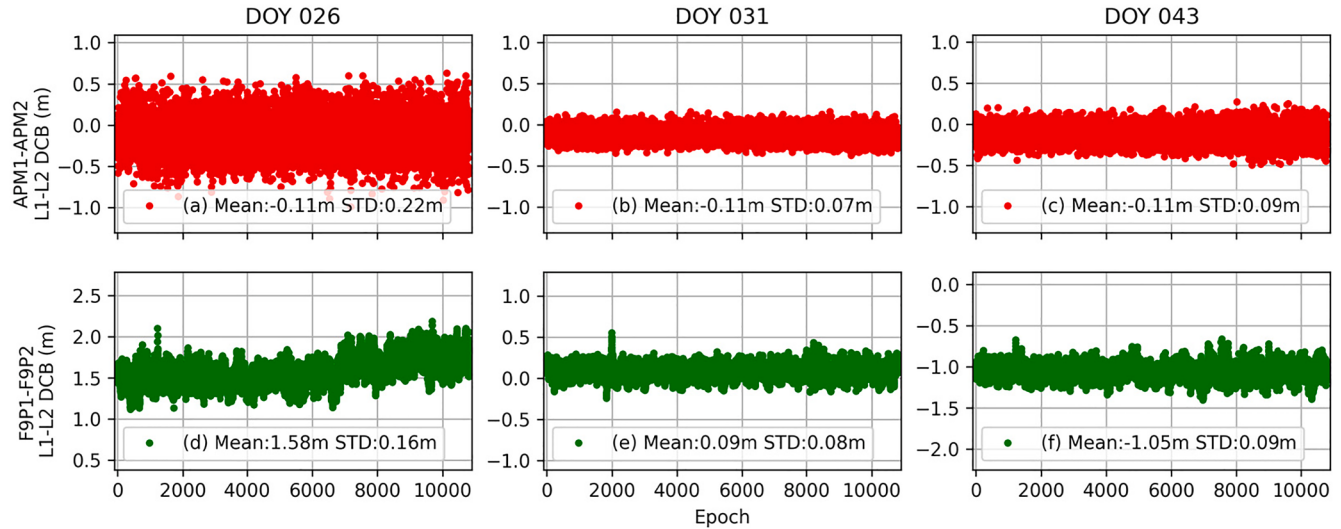


Fig. 5. DCB between L1 and L2 of GPS for the APM1-APM2 pair (top) and the F9P1-F9P2 pair (bottom) on DOYs 26, 31 and 43 of 2022.

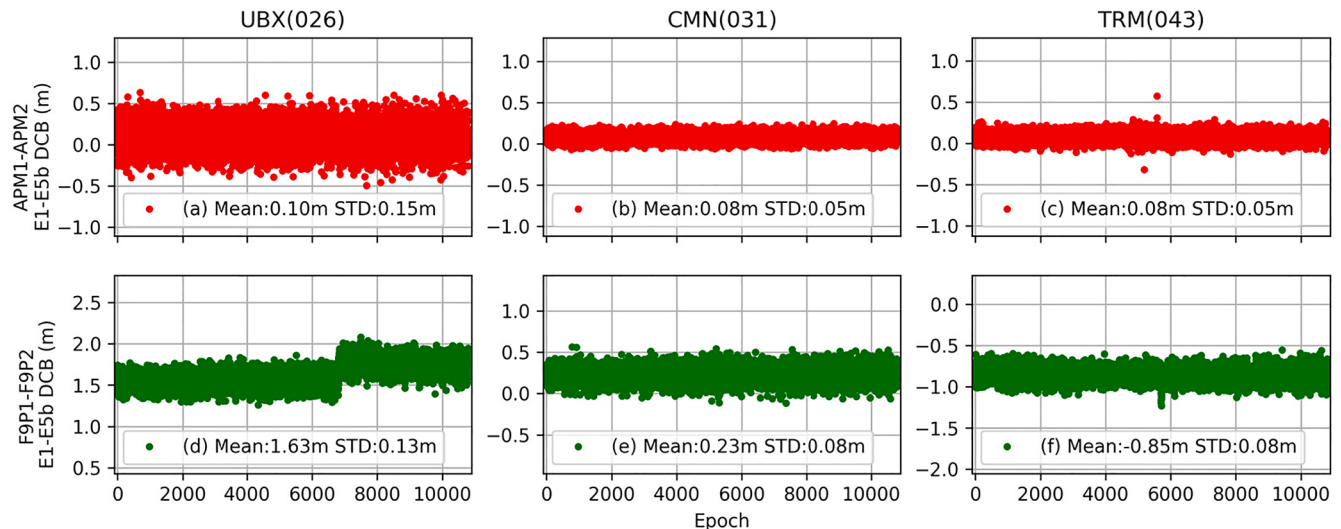


Fig. 6. DCB between E1 and E5b of Galileo for the APM1-APM2 pair (top) and the F9P1-F9P2 pair (bottom) on DOYs 26, 31 and 43 of 2022.

**Table 4**

Mean and STD of the DCB between L1 and L2 and the DCB between E1 and E5b of the zero-length baseline APM1-APM2 (Trimble Alloy receivers pair) and zero-length baseline F9P1- F9P2 (U-blox C099-F9P receivers pair) on DOYs 026, 031 and 043 in 2022.

Baseline	DOY	L1-L2 DCB (m)		E1-E5b DCB (m)	
		Mean	STD	Mean	STD
APM1-APM2	026 (UBX)	-0.106	0.221	0.096	0.149
	031 (CMN)	-0.109	0.071	0.084	0.046
	043 (TRM)	-0.115	0.094	0.078	0.051
F9P1-F9P2	026 (UBX)	1.585	0.160	1.629	0.129
	031 (CMN)	0.091	0.078	0.231	0.084
	043 (TRM)	-1.052	0.089	-0.852	0.076

decrease when the receiver is equipped with a good antenna. Second, the stability of the DPB estimates for the zero-length baseline case is apparent on both the Trimble Alloy or U-blox C099-F9P receivers. The U-blox C099-F9P receivers can achieve the same level of DPB estimate accuracy as the Trimble receivers.

The DPB of the Trimble receivers is smaller than the DPB of the U-blox receivers. However, the DPB STDs are all smaller than 0.007 cycles. Combined with the DPB characteristics, this can be attributed to the fact that the L1-L2 and E1-E5b DPB of the receivers involved in the experiment are all stable. The short-term temporal characteristics of the L1-L2 and E1-E5b DPB are similar, regardless of whether APM1-APM2 or F9P1-F9P2 pairs are used, which helps us realize that the quality of phase observables from low-cost receivers can be treated equally to the phase observables of high-grade receivers. Based on this, we may

develop a phase-only model to obtain a high-precision solution using low-cost receivers in the future. For the PB, we first recall the PB formula and use GPS as an example:  $\tilde{\delta}_1^G = (\lambda_1^G \delta_1^G - d_1^G + \lambda_1^G a_1^{1g}) / \lambda_1^G$ . In our model, we assume that  $\lambda_1^G \delta_1^G$  absorb  $d_1^G$  and  $\lambda_1^G a_1^{1g}$ .  $d_1^G$  is the receiver code hardware delay at the first frequency, which is a real value and related to the hardware, so it should be measured exactly and analyzed, especially in low-cost receivers. When  $\lambda_1^G a_1^{1g}$  is considered invariant over a short time, the character of  $\lambda_1^G \delta_1^G$  will be driven by  $d_1^G$ , since  $\lambda_1^G \delta_1^G$  varies less than  $d_1^G$ . To compare the GPS and Galileo phase biases on the same scale, the PB estimates should be multiplied by the wavelength of the second frequency in the corresponding systems to unify the unit (m).

Different from the DPB, the impact of the antenna on  $d_1^G$  can be observed. The result shows that the signal distortion biases at the antenna end are notable. When we compare the three APM1-APM2 datasets in Fig. 11, the PB STDs of the receiver connected to the ANN-MB antenna are approximately two times that of the receiver connected to the Trimble Choke Ring antenna. The Galileo schemes also support it in Fig. 12. The PB STDs of the F9P receivers connected to the ANN-MB antenna show lower noise than that of the Trimble receivers, while the PB STDs of the C099-F9P receivers connected to the other antennas show larger noise than that of the Trimble receivers. The Galileo PB STDs are all smaller than the GPS PB STDs. The results are consistent with the statement that Galileo has a better pseudorange observation, which has been proven by previous research.

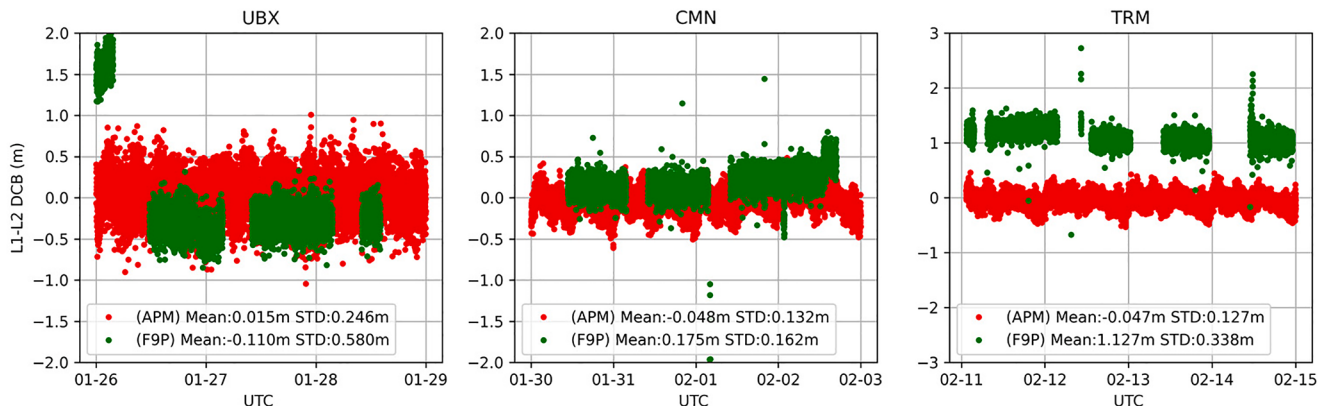


Fig. 7. DCB between L1 and L2 of GPS for the APM1-APM2 pair (red) and the F9P1-F9P2 pair (green) on DOYs 26–28, 30–33 and 42–45 of 2022.

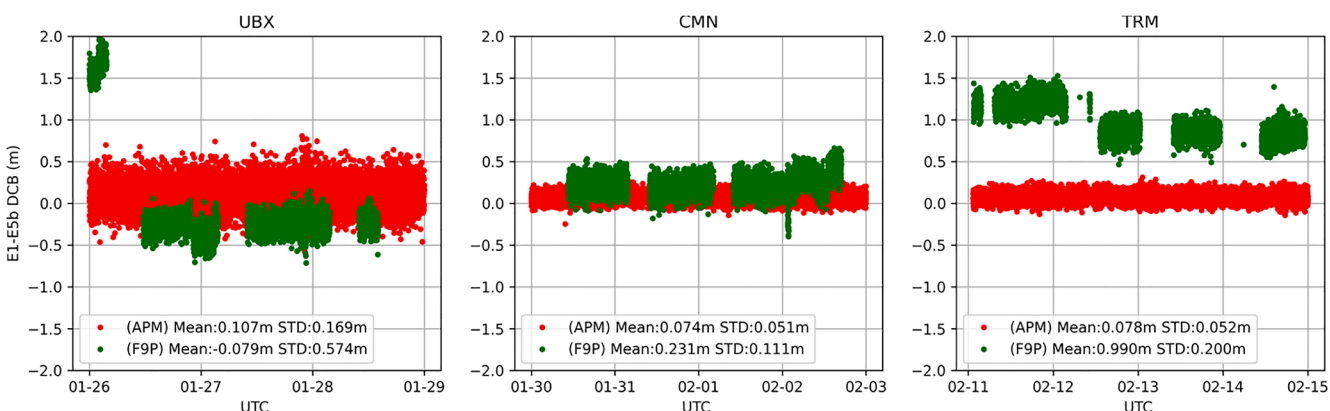
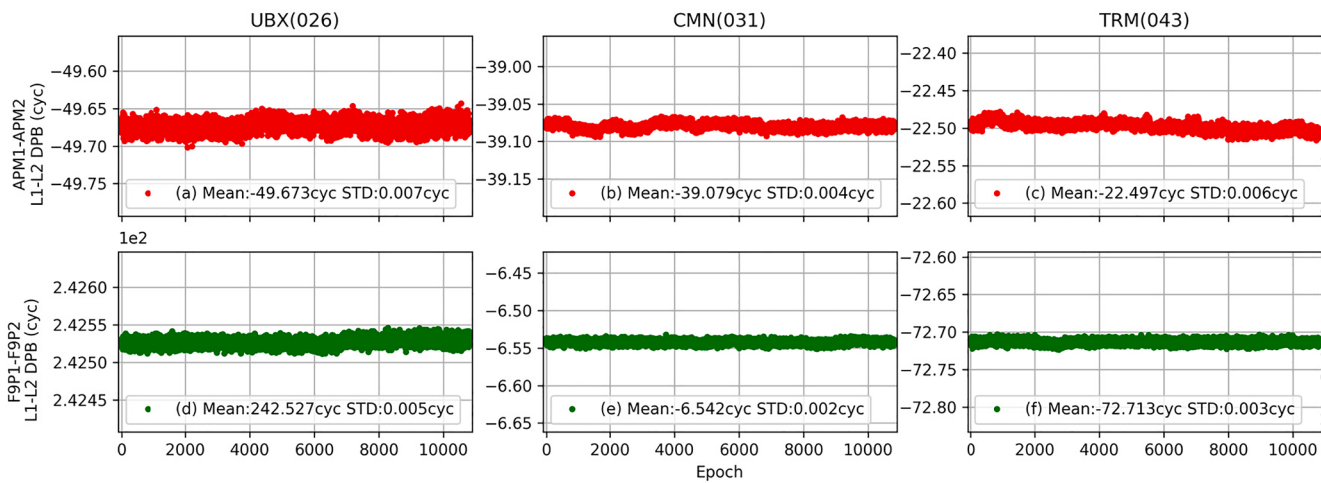
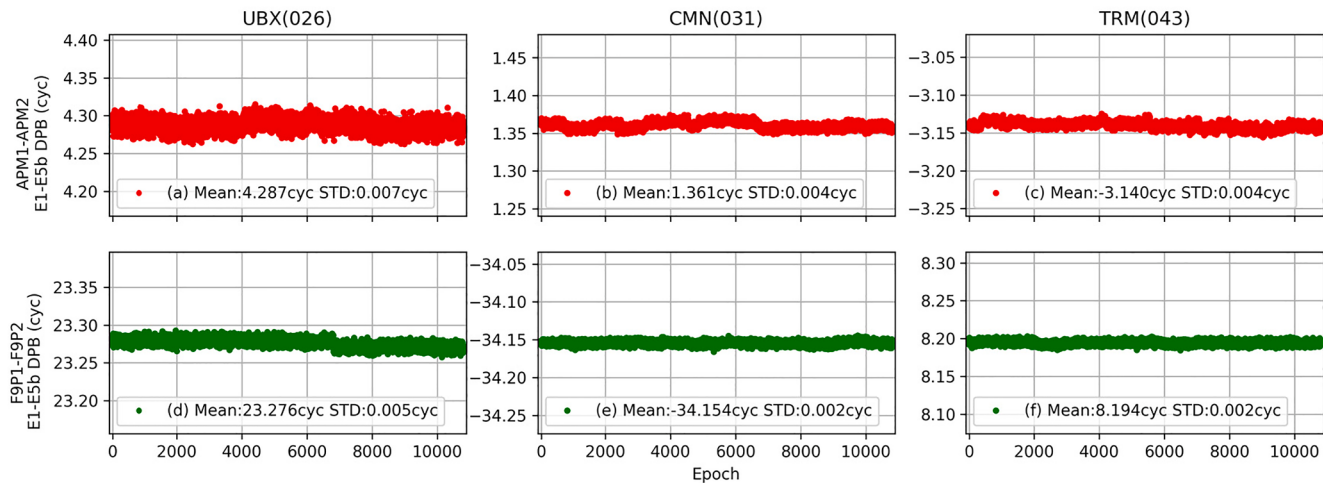


Fig. 8. DCB between E1 and E5b of Galileo for the APM1-APM2 pair (red) and the F9P1-F9P2 pair (green) on DOYs 26–28, 30–33 and 42–45 of 2022.



**Fig. 9.** DPB between L1 and L2 of GPS for the APM1-APM2 pair (top) and the F9P1-F9P2 pair (bottom) on DOYs 26, 31 and 43 of 2022.



**Fig. 10.** DPB between E1 and E5b of Galileo for the APM1-APM2 pair (top) and the F9P1-F9P2 pair (bottom) on DOYs 26, 31 and 43 of 2022.

**Table 5**

Mean and STD of the DPB (cycle) between L1 and L2 and the DPB (cycle) between E1 and E5b of APM1-APM2 (Trimble Alloy receivers pair) and F9P1-F9P2 (U-blox C099-F9P receivers pair) on DOYs 026, 031 and 043 in 2022.

Baseline	DOY	L1-L2 DPB (cycle)		E1-E5b DPB (cycle)	
		Mean	STD	Mean	STD
APM1-APM2	026 (UBX)	49.673	0.007	4.287	0.007
	031 (CMN)	4.287	0.004	1.361	0.004
	043 (TRM)	-22.497	0.006	-3.140	0.004
F9P1-F9P2	026 (UBX)	242.527	0.005	23.276	0.005
	031 (CMN)	-6.542	0.002	-34.154	0.002
	043 (TRM)	-72.713	0.003	-8.194	0.002

### 3.4. RTK position performance

To intuitively compare the RTK positioning performance of the float and fixed solutions under six different circumstances and illustrate that the proposed method can improve the function model's performance, the results of the APM1-APM2 and F9P1-F9P2 baselines on DOYs 026, 031, and 042 of 2022 are reported. Figs. 13 and 14 show the positioning results based on the float solutions from the low-cost and high-grade receivers for horizontal position scatters under three typical scenarios. These results were obtained by comparing the estimated positions to precise benchmark coordinates obtained by the CSRS service using a

GPS-only PPP-AR strategy. The statistical results of the float solution position performance in the east, north and up directions under the six different circumstances are presented in Table 6.

According to the results shown in Table 6, a survey-grade antenna can significantly improve the performance of low-cost receivers, making the code and phase noise estimates more similar to those of high-grade receivers. It is concluded that survey-grade antennas are sufficient for survey tasks using low-cost receivers to obtain better performance from the perspective of RRB characters because the hardware noise can be reduced. It should be noted that we should also take their multipath inhibition effect into consideration when we choose antennas. The characteristics of the observables and positioning results are affected by the joint effect of receiver hardware and the external antenna. The position performances with the Trimble receiver + U-blox ANN-MB combination show worse performance than the C099-F9P + U-blox ANN-MB combination among the six combinations. The precision of the float solutions is dependent on the function model and the quality of the phase + code observables. Low-cost receivers connected to a Trimble GNSS-Ti Choke Ring antenna can achieve a horizontal position accuracy similar to Trimble receivers + Comnav AT360 antenna. We have thus illustrated that a low-cost receiver solution still has the potential to perform very well and achieve the same positioning accuracy level that high-grade receivers can obtain. Once the quality of an external antenna is improved, the position components following the distribution of the

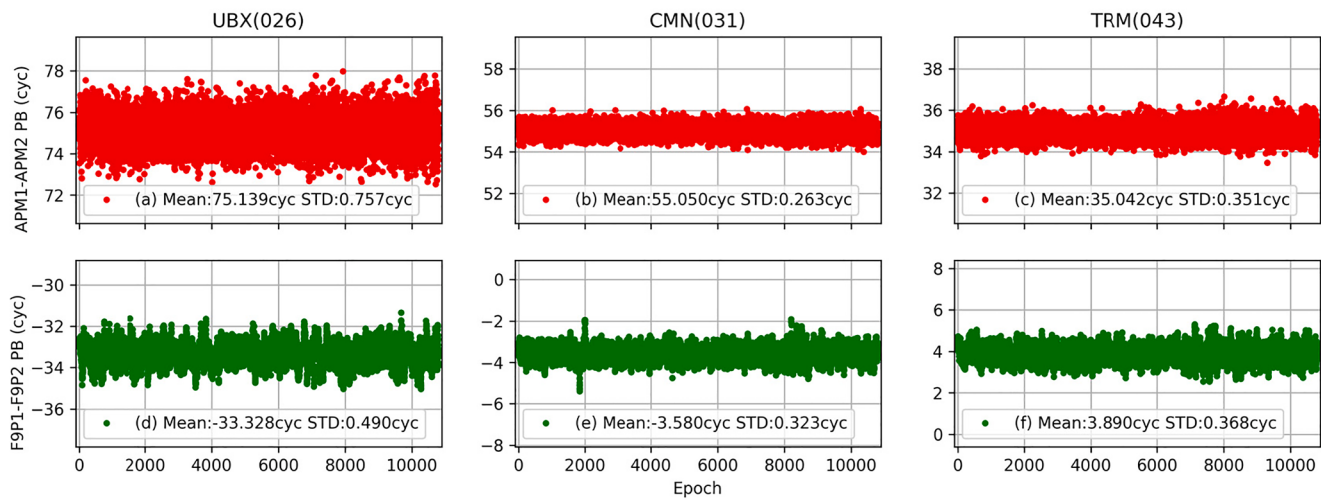


**Fig. 11.** PB at the GPS L1 frequency for the APM1-APM2 pair (top) and the F9P1-F9P2 pair (bottom) on DOYs 26, 31 and 43 of 2022.

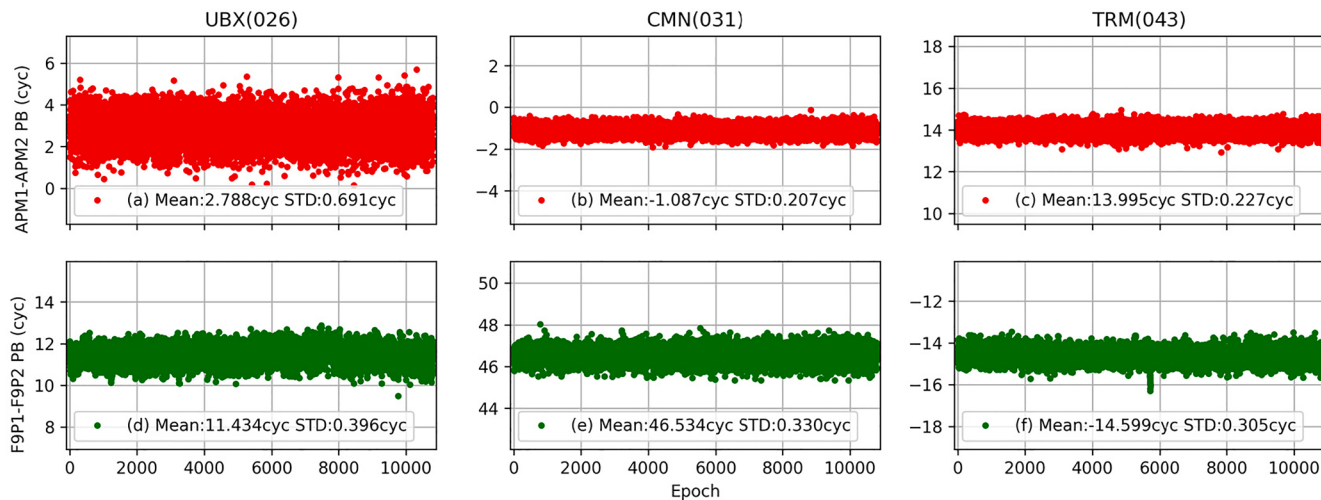


**Fig. 12.** PB at the Galileo E1 frequency for the APM1-APM2 pair (top) and the F9P1-F9P2 pair (bottom) on DOYs 26, 31 and 43 of 2022.

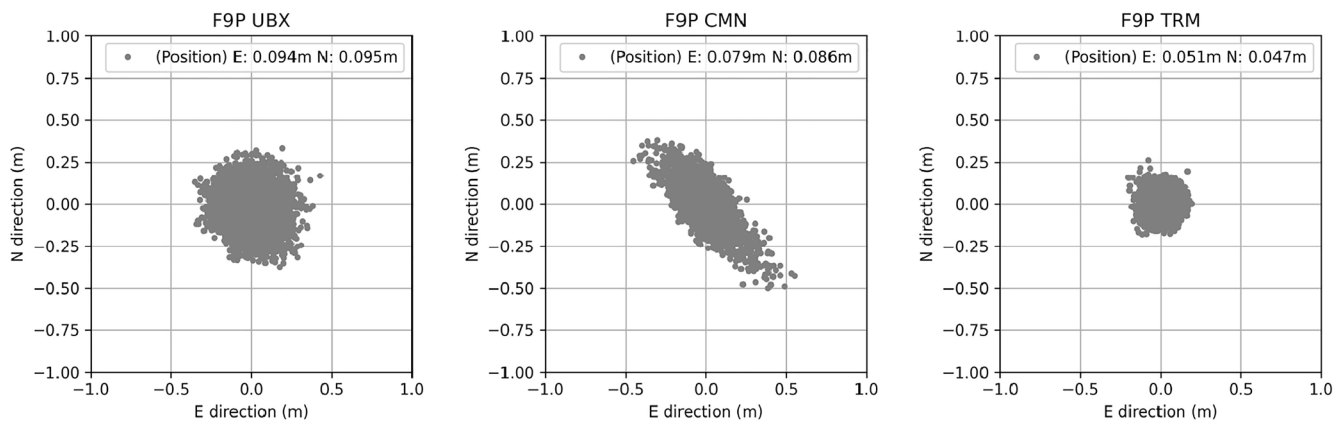


**Fig. 13.** Single-differenced RTK position performance of the float solutions for the F9P1-F9P2 zero-length baseline on DOYs 026, 031 and 042 of 2022.

error ellipse can be observed.

For the fixed solutions, we compare the position performance results with fixed ambiguities in Figs. 15 and 16, the corresponding statistical results of the fixed solution is presented in Table 7. The ambiguity-fixed position precisions are mainly dependent on the quality of the phase

observables and the function model. We found that the F9P1-F9P2 result is comparable to that of the APM1-APM2 result. We proved that it is feasible to obtain precise solutions in a low-cost relative positioning mode with fixed ambiguities. Such results move us toward a collaborative precise positioning with low-cost receivers.

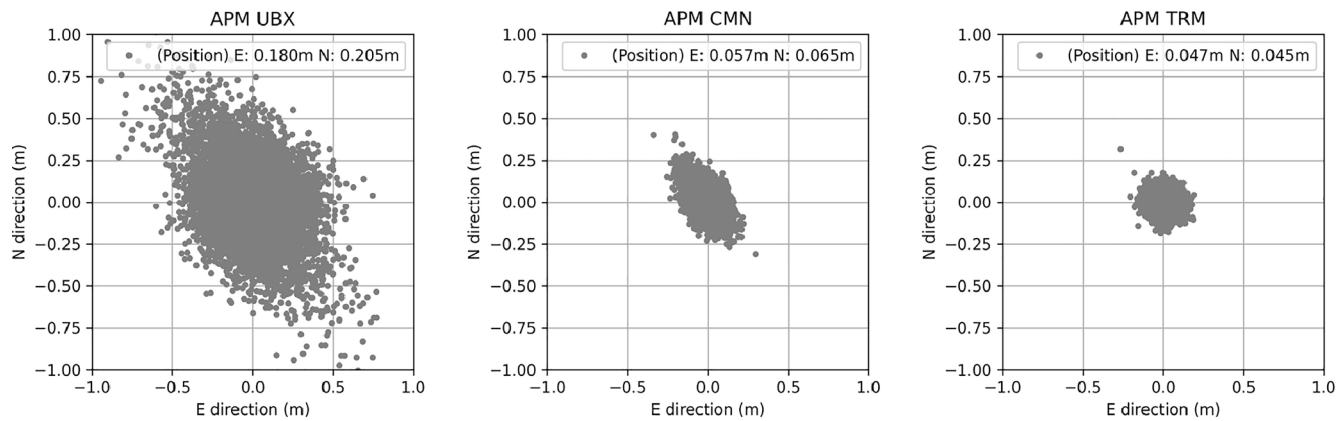


**Fig. 14.** Single-differenced RTK position performance of the float solutions for the APM1-APM2 zero-length baseline on DOYs 026, 031 and 042 of 2022.

**Table 6**

Statistical results of the positioning performance of the float solutions from the F9P1-F9P2 and APM1-APM2 zero-length baselines on DOYs 026, 031 and 043 of 2022.

Baseline	DOY	Antenna type	Position performance (mm)		
			E	N	U
F9P1-F9P2	026 (UBX)	U-blox ANN-MB	9.43	9.53	25.52
	031 (CMN)	Comnav AT360	7.89	8.64	21.53
	043 (TRM)	Trimble GNSS-Ti Choke Ring	5.06	4.74	15.92
APM1- APM2	026 (UBX)	U-blox ANN-MB	18.02	20.52	47.42
	031 (CMN)	Comnav AT360	5.65	6.54	13.96
	043 (TRM)	Trimble GNSS-Ti Choke Ring	4.74	4.48	15.19

#### 4. Conclusion

This study addressed a scientific question regarding the characters of RRB on low-cost and geodetic GNSS observables when connected to different grades of antennas. Specifically, a geometry-based model is deduced. It is crucial to estimate systematic errors, including the DCB, ISB and DPB. Some parameters are chosen as a datum and reparameterized for solving the problem of rank deficiency. After that, a LSF method is adopted to enable the subsequent DPB estimation. We conducted a comparative analysis of RRB from the low-cost and geodetic

receivers, including the clock offset, ISB, DCB, DPB and PB from short-term and long-term scales. Finally, the SD RTK position performances of the two types of receivers were assessed using different grades of antennas. We found that should the RRB depend on the receivers' hardware. Apart from RRB itself, the noise of RRB exists on observables and is also important for stochastic modeling when removing or reducing RRB with correction, which is related to the hardware and antenna. The main concluding remarks and main contributions of this work are as follows:

- (1) We reported an abnormal phenomenon in which the C099-F9P receiver showed better performance than the Trimble receiver on signal quality and RRB when the U-blox ANN-MB antenna was used.
- (2) Low-cost receivers are comparable to high-grade receivers in terms of RRB and position performance when equipped with a survey-grade or higher-grade antenna.
- (3) As for receiver-related biases, it is obvious that a low-cost antenna will introduce additional noise to the observables and have a negative impact on the ISB. It should be noted that the L1-L2 and E1-E5b DCB will change when low-cost receivers restart or power off. When connected to a higher-grade antenna, low-cost receivers can show DCB estimate stability similar to Trimble receivers over a short period. The DCB STD of low-cost receivers can reach 0.076 m. The DPB of low-cost receivers shares the same stability as Trimble receivers, the STD of which can reach approximately 0.003 cycles. Because the phase observables have comparable accuracy, the implementation of a phase-only method can be free from noise in the code observables.

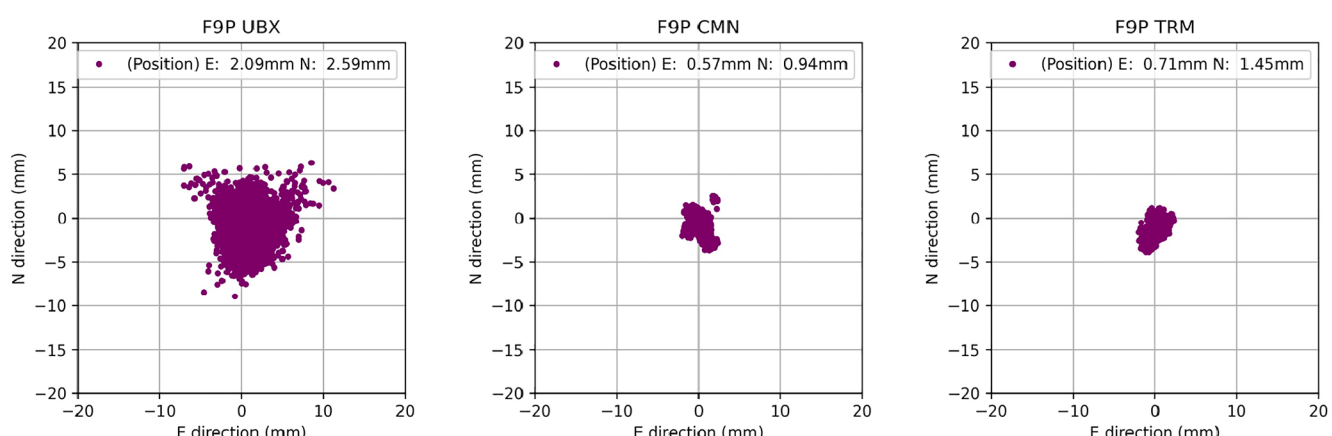


**Fig. 15.** Single-differenced RTK position performance of the fixed solutions for the F9P1-F9P2 zero-length baseline on DOYs 026, 031, and 042 of 2022.

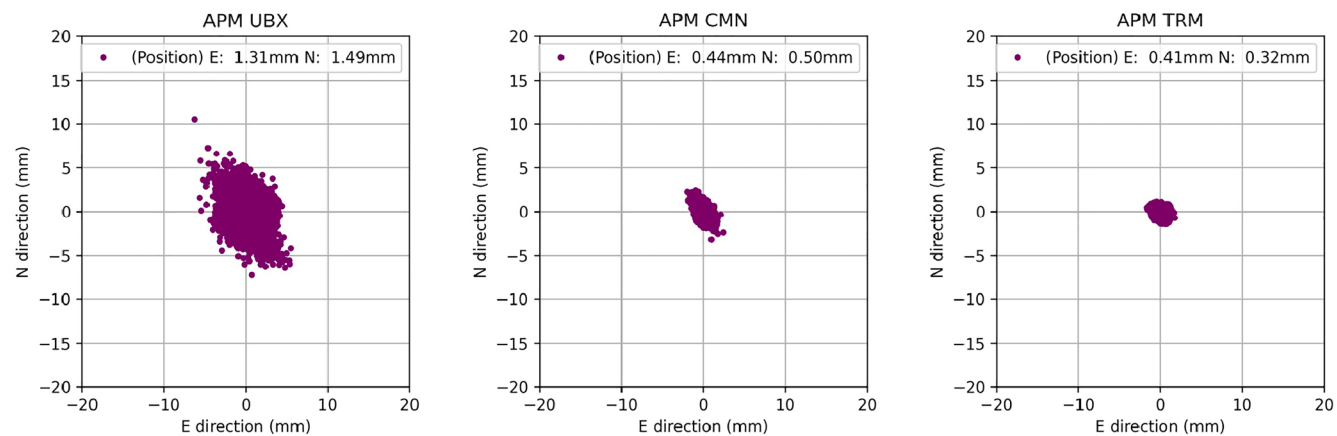


**Fig. 16.** Single-differenced RTK position performance of the fixed solutions for the APM1-APM2 zero-length baseline on DOYs 026, 031, and 042 of 2022.

**Table 7**

Statistical results of the positioning performance of the correctly fixed solutions under the six different circumstances.

Baseline	DOY	Antenna type	Position performance (mm)		
			E	N	U
APM1-APM2	026 (UBX)	U-blox ANN-MB	1.322	1.488	3.204
	031 (CMN)	Comnav AT360	0.437	0.504	1.056
	043 (TRM)	Trimble GNSS-Ti Choke Ring	0.407	0.322	1.087
F9P1-F9P2	026 (UBX)	U-blox ANN-MB	2.094	2.594	4.730
	031 (CMN)	Comnav AT360	0.567	0.942	1.140
	043 (TRM)	Trimble GNSS-Ti Choke Ring	0.727	1.525	1.201

- (4) For positioning performance, the float solutions from the C099-F9P receivers connected to a Trimble GNSS-Ti Choke Ring antenna can reach accuracies of 5.06, 4.74 and 15.92 mm in the east, north and up directions, respectively. The results are 46%, 50% and 37% improvements compared to the ANN-MB antenna case. The position accuracy of the fixed solutions from the low-cost receiver is worse than that of high-grade receivers, but it is sufficient for cm-level positioning using low-cost receivers.
- (5) The proposed method is also rigorous and effective. It is based on a full-rank functional model and a LSF method, making it possible to analyze and model the RRB of low-cost receivers, which is forward-looking work.

Finally, it is anticipated that low-cost receivers can achieve similar level and capability with high-grade receivers in positioning services when a survey-grade or higher-quality antenna is equipped and the RRB and functional models are refined or handled well. In the future, an increasing number of low-cost receivers will become a valid complement to geodetic receivers for public PNT services.

#### CRediT authorship contribution statement

**Luohong Li:** Conceptualization, Data curation, Formal analysis, Review & editing. **Yunbin Yuan:** Project administration, Resources, Software, Supervision, Review & editing. **Pengfei Zhang:** Formal analysis, Visualization, Review & editing.

#### Declaration of Competing Interest

The authors declare that they have no known competing financial interests or personal relationships that could have appeared to influence the work reported in this paper.

#### Data availability

The authors do not have permission to share data.

#### Acknowledgments

This research was jointly funded by the National Key Research Program of China: ‘Collaborative Precision Positioning Project’ (No. 2016YFB0501900) and the National Natural Science Foundation of China (No. 42074045, No. 42004022). We offer many thanks to the IGS MGEX for providing the multi-GNSS broadcast ephemeris. We also thank Natural Resources Canada for the CSRS online PPP-AR service. Thank Dr. Yang Zhouming for the advice on the figure plotting and text format in this work.

#### References

- [1] G.W. Hein, Status, perspectives and trends of satellite navigation, *Satellite Navigation* 1 (2020) 22.
- [2] R. Odolinski, P. Teunissen, On the performance of a low-cost single-frequency GPS +BDS RTK positioning model. 2017 International Technical Meeting of The Institute of Navigation, 2017.
- [3] P. Zhou, Low-Cost Real-Time Precise Point Positioning (PPP), Correction Service with High Availability and Accuracy (2020).
- [4] M.J. Wouters, Evaluation Of A New Low-Cost Receiver for GNSS Time-Transfer, 2021 Joint Conference of the European Frequency and Time Forum and IEEE International Frequency Control Symposium (EFTF/IFCS), 2021, pp. 1-4.
- [5] E. Benedetti, A. Dermani, M. Crespi, On the feasibility to integrate low-cost MEMS accelerometers and GNSS receivers, *Adv. Space Res.* 59 (2017) 2764–2778.
- [6] C. Xue, P.A. Psimoulis, X. Meng, Feasibility analysis of the performance of low-cost GNSS receivers in monitoring dynamic motion, *Measurement* (2022).
- [7] C. Zhao, Y. Yuan, B. Zhang, M. Li, Ionosphere Sensing With a Low-Cost, Single-Frequency, Multi-GNSS Receiver, *IEEE Trans. Geosci. Remote Sens.* 57 (2019) 881–892.
- [8] C. Zhao, B. Zhang, W. Li, Y. Yuan, M. Li, Simultaneous Retrieval of PWV and VTEC by Low-Cost Multi-GNSS Single-Frequency Receivers, *Earth and Space, Science* 6 (2019) 1694–1709.
- [9] C. Zhao, B. Zhang, R. Odolinski, Y. Yuan, Combined use of single-frequency data and global ionosphere maps to estimate BDS and Galileo satellite differential code biases, *Meas. Sci. Technol.* 31 (2020).
- [10] M.J. Murrian, C.W. Gonzalez, T.E. Humphreys, T.D. Novlan, A dense reference network for mass-market centimeter-accurate positioning, *IEEE/ION Position Location Navigation Symposium (PLANS) 2016* (2016) 243–254.
- [11] K. Stępniaik, J. Paziewski, On the quality of tropospheric estimates from low-cost GNSS receiver data processing, *Measurement* 198 (2022).
- [12] Z. Zhang, H. Yuan, B. Li, X. He, S. Gao, Feasibility of easy-to-implement methods to analyze systematic errors of multipath, differential code bias, and inter-system bias for low-cost receivers, *GPS Solutions* 25 (2021).

- [13] H. Yuan, Z. Zhang, X. He, G. Li, S. Wang, Stochastic model assessment of low-cost devices considering the impacts of multipath effects and atmospheric delays, *Measurement* 188 (2022).
- [14] B. Zhang, C. Zhao, R. Odolinski, T. Liu, Functional model modification of precise point positioning considering the time-varying code biases of a receiver, *Satellite Navigation* 2 (2021).
- [15] X. Mi, B. Zhang, Y. Yuan, X. Luo, Characteristics of GPS, BDS2, BDS3 and Galileo inter-system biases and their influence on RTK positioning, *Meas. Sci. Technol.* 31 (2020).
- [16] C.Z. Yong, R. Odolinski, S. Zaminpardaz, M. Moore, E. Rubinov, J. Er, M. Denham, Instantaneous, Dual-Frequency, Multi-GNSS Precise RTK Positioning Using Google Pixel 4 and Samsung Galaxy S20 Smartphones for Zero and Short Baselines, *Sensors* (Basel) 21 (2021).
- [17] C. Zhao, B. Zhang, X. Zhang, SUPREME: an open-source single-frequency uncombined precise point positioning software, *GPS Solutions* 25 (2021).
- [18] J.A. Momoh, S. Bhattacharai, M. Ziebart, Receiver clock jump and cycle slip correction algorithm for single-frequency GNSS receivers, *GPS Solutions* 23 (2019).
- [19] X. Gong, F. Zheng, S. Gu, Z. Zhang, Y. Lou, The long-term characteristics of GNSS signal distortion biases and their empirical corrections, *GPS Solutions* 26 (2022).
- [20] X. Mi, B. Zhang, Y. Yuan, Stochastic modeling of between-receiver single-differenced ionospheric delays and its application to medium baseline RTK positioning, *Meas. Sci. Technol.* 30 (2019).
- [21] G. Falco, M. Pini, G. Marucco, Loose and Tight GNSS/INS Integrations: Comparison of Performance Assessed in Real Urban Scenarios, *Sensors* (Basel) 17 (2017).
- [22] G. Li, J. Wu, C. Zhao, Y. Tian, Double differencing within GNSS constellations, *GPS Solutions* 21 (2017) 1161–1177.
- [23] W. Liu, M. Wu, X. Zhang, W. Wang, W. Ke, Z. Zhu, Single-epoch RTK performance assessment of tightly combined BDS-2 and newly complete BDS-3, *Satellite Navigation* 2 (2021).
- [24] Y. Tian, L. Sui, G. Xiao, D. Zhao, H. Chai, C. Liu, Estimating inter-system biases for tightly combined Galileo/BDS/GPS RTK, *Adv. Space Res.* 65 (2020) 572–585.
- [25] W. Zhao, G. Liu, M. Gao, D. Lv, R. Wang, INS-assisted inter-system biases estimation and inter-system ambiguity resolution in a complex environment, *GPS Solutions* 27 (2022).
- [26] M. Li, Y. Yuan, N. Wang, T. Liu, Y. Chen, Estimation and analysis of the short-term variations of multi-GNSS receiver differential code biases using global ionosphere maps, *J. Geod.* 92 (2017) 889–903.
- [27] J. Zha, B. Zhang, Y. Yuan, X. Zhang, M. Li, Use of modified carrier-to-code leveling to analyze temperature dependence of multi-GNSS receiver DCB and to retrieve ionospheric TEC, *GPS Solutions* 23 (2019).
- [28] C.B. Zhao, B.C. Zhan, R. Odolinski, Y.B. Yuan, Combined use of single-frequency data and global ionosphere maps to estimate BDS and Galileo satellite differential code biases, *Meas. Sci. Technol.* 31 (2020).
- [29] Y. Yuan, X. Mi, B. Zhang, Initial assessment of single- and dual-frequency BDS-3 RTK positioning, *Satellite Navigation* 1 (2020).
- [30] R. Odolinski, P.J.G. Teunissen, D. Odijk, Combined BDS, Galileo, QZSS and GPS single-frequency RTK, *GPS Solutions* 19 (2014) 151–163.
- [31] X. Mi, B. Zhang, R. Odolinski, Y. Yuan, On the temperature sensitivity of multi-GNSS intra- and inter-system biases and the impact on RTK positioning, *GPS Solutions* 24 (2020).
- [32] P.J.G. Teunissen, The least-squares ambiguity decorrelation adjustment: a method for fast GPS integer ambiguity estimation, *J. Geodesy* 70 (1995) 65–82.
- [33] E. Mysen, Erratum to: On the equivalence of Kalman filtering and least-squares estimation, *J. Geod.* 91 (2017) 463.
- [34] B. Zhang, P.J.G. Teunissen, Y. Yuan, On the short-term temporal variations of GNSS receiver differential phase biases, *J. Geod.* 91 (2016) 563–572.
- [35] B. Zhang, P.J.G. Teunissen, Y. Yuan, H. Zhang, M. Li, Joint estimation of vertical total electron content (VTEC) and satellite differential code biases (SDCBs) using low-cost receivers, *J. Geod.* 92 (2017) 401–413.
- [36] B. Zhang, P.J.G. Teunissen, Y. Yuan, X. Zhang, M. Li, A modified carrier-to-code leveling method for retrieving ionospheric observables and detecting short-term temporal variability of receiver differential code biases, *J. Geod.* 93 (2018) 19–28.